Pergamon

Int. J. Impact Engng. Vol. 17, pp. 751–762, 1995

0734-743X/95 $9.50+0.00

HYPERVELOCITY IMPACT ON LAMINATE COMPOSITE PANELS

V.V.Silvestrov, A.V.Plastinin and N.N.Gorshkov

Laboratory of High Velocity Processes, Lavrentyev Institute of Hydrodynamics,
Siberian Division of Russian Academy of Sciences, Lavrentyev Avenue 15, Novosibirsk 630090, Russia

Summary—Phenomenological results on the damage of flat glass-, aramid- and carbon-fiber reinforced epoxy laminated composites under the impact of steel and glass projectiles at velocity up to 8–11 km/s are presented. The damage of composite panels under hypervelocity impact is shown to differ significally from that observed for elastoplastic materials. However, it is shown that a number of qualititative results may be adequately described by the empirical dependences established earlier for metals.

INTRODUCTION

Application of composites for space is constantly widening. On orbit, the elements made of composites may be impacted by solid particles of meteorites or cosmic debris moving with space velocities. This necessitates the investigation of hypervelocity impact on composites [1]. The destruction of composite structures under hypervelocity impact of solid particles was studied earlier in the regime of through perforation by aluminium and nylon projectiles: the destruction of panels [2] and carbon/epoxy tubes [3], protecting properties of kevlar and carbon/epoxy shields [4]. It was shown that large damage zones emerge at the surface under hypervelocity impact due to laminated structure of the composites.

This paper is intended to consider the effect of hypervelocity impact on the targets of some typical laminated composites as compared to metallic ones. For this purpose the limit perforation thickness and the size of craters under impact on semi-infinite targets, as well as the dependence of these values on the projectile velocity and material properties were determined. On the basis of present knowledge on the hypervelocity impact on elastic-plastic materials it is obvious that the results obtained for semi-infinite targets may serve as a basis for understanding the penetration mechanics and modeling the crater formation (when the phenomenon is not complicated by the effect of rarefaction waves from the back side of the target, and the considerable part of projectile kinetic energy is absorbed by the target).

TARGETS AND PROJECTILES

The main part of the results are obtained for glass-cloth-base-laminate STEF. The data for the other composites made it possible to supplement and extend the qualitative conclusions following from the results for STEF. Four materials (three composites and an unreinforced epoxy resin matrix) were used as targets :

– *Glass-cloth-base composite.* Flat targets were cut from electrical engineering glass-cloth-base-laminate (textolite) of two types: STEF and ST-1 with identical reinforcement structure

(base - straw glass cloth of linen weave, up to 50 % of volume), but with other matrix material: epoxy resin for STEF and phenol-formaldehyde resin for ST-1, and other thickness of the glass fabric. Since another type of resin and thinner reinforcing cloth are used in ST-1, its strength characteristics are 2–3 times lower than those of STEF. Both materials are laminated, the thickness of the layers being approximately 0.1–0.3 mm. The mass density of the composites is ρ_t = 1.71 g/cc and 1.85 g/cc , Brinell hardness H_B is 360 MPa and 630 MPa for ST-1 and STEF, respectively. The thickness of targets varied from 10 to 30 mm, area 10 × 10 cm^2. For this thickness no damage of the material is observed at/near the back surface of the targets.

– *Aramid-fiber/epoxy composite.* Target lay–up utilized unidirectional fiber plys $(\pm 60, 0, 90, \pm 60)\,nr$, and an epoxy resin matrix resulting in an overall material density of ρ_t = 1.29 g/cc. The thickness of a single ply is 0.7 mm, while the target thickness is 30 mm, and the area is 20 × 20 cm^2.

– *Carbon-fiber/epoxy composite.* Target lay–up utilized unidirectional fiber plys $(\pm 45)\,nr$, and an epoxy resin matrix resulting in an overall material density of ρ_t = 1.41 g/cc. The thickness of one ply is 0.5 mm, while the target thickness is 8 mm, and the area is 40 × 10 cm^2.

– *Epoxy.* The samples of cast epoxy were used to obtain baseline impact results for matrix material. Their density was 1.2 g/cc, diameter was 12 cm, the thickness was 5 cm.

Projectiles. The balls are steel (density ρ = 7.8 g/cc, with final diameter d = 0.53 to 4.5 mm) and optical glass (ρ = 2.7 g/cc, d = 1.3 to 2.3 mm) and were accelerated up to v = 11.2 km/s and 7.8 km/s, respectively, using the tubular high explosive accelerator [5].

PERFORATION LIMIT FOR GLASS-CLOTH-BASE COMPOSITE

Figure 1 presents the qualitative cross-sectional drawing of the damage structure in perforated

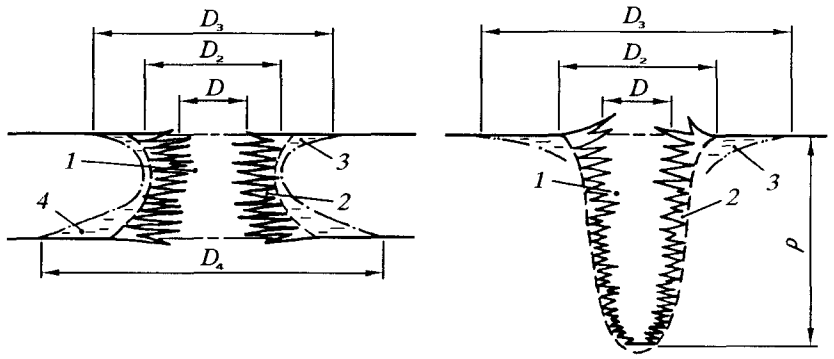

(a) (b)

Fig. 1. The drawing of the crater structure in perforated (a) and semi-infinite (b) composite targets. 1 – cavern, 2 – zone of partial damage, 3, 4 – front and back "whitening" zones.

and non-perforated semi-infinite composite targets. In both cases there is quasi-cylindrical zone 1 – *hole* (Fig. 1a) or *cavern* (Fig. 1b) – in the center of the crater structure. In this zone the target material is completely destructed and is ejected out. The inner lateral surface of the hole or cavern in composites is uneven, since it is formed by pouring out of a portion of matrix material and multiple breakages and delamination of reinforced filaments. The photographs of the target cross-sections are presented in Fig. 2. For the above reasons accurate measurements of the hole or cavern diameter D are infeasible, it may be estimated only. However, the penetration depth p measured from the level of initial target surface is determined to the accuracy of $\sim$ 0.1–0.2 mm.

In addition to the cavern (or hole) there are two other, visually observed damage zones on the STEF-target crater cross-section (Fig. 1b). The first surrounds the cavern, and matrix material in this zone 2 is pierced by a network of cracks and partially damaged. Its diameter is 2–4 times larger than the cavern (or hole) diameter and its contour is similar to the crater form for elastic materials, which reflects the quasi-spherical symmetry of the process of shock-wave

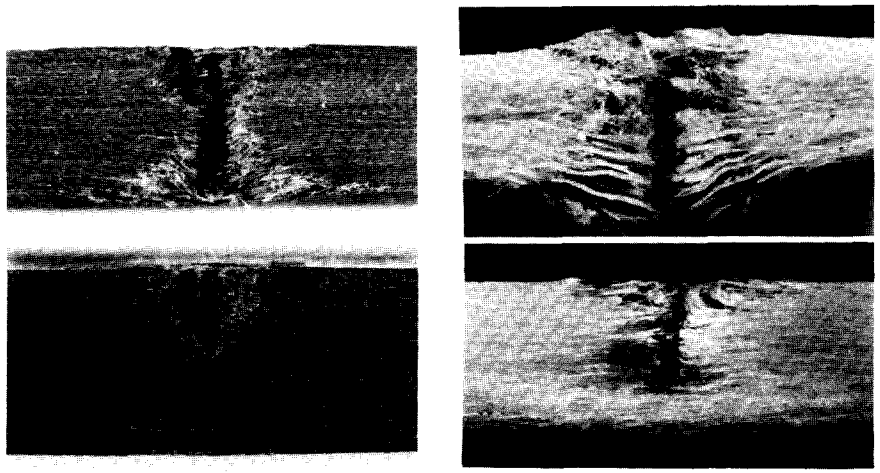

(a) (b)

Fig. 2. Target cross-sections near the limit perforation for ST-1 (a) and STEF (b).
(a) – steel projectile – 4.8 km/s, 1.1 mm; (b) – glass projectile – 7.8 km/s, 1.3 mm; target thickness in mm (from up to down): (a) – 8.8, 11; (b) – 4.0, 4.8

flow. This zone emerges due to the energy dissipation of the penetrating projectile in the target material nearby the cavern surface up to its complete consuming or stopping.

The next zones 3 and 4 are limited by the "whitening" contour on the target surfaces. They are connected with the effect of compression wave diverging from the impact point and conical rarefaction waves from the side of target surfaces on the target material. On the whole the material in these zones preserves its continuity. But there are the local "whitening" and small cracks indicating the partial disturbance of the matrix continuity. These zones are likely to be the analog of the zone of deformation propagation around the crater studied for cooper targets [10]. For the opaque ST-1 textolite, organic and carbon plastics the zones 3 and 4 are not observed visually.

The limit perforation thickness was determined for glass-cloth-base-composite for normal impact by steel and glass projectiles. Figure 3 presents initial data: along the horizontal axis – relative target thickness t/d, along the vertical – penetration depth p/d. If the target is

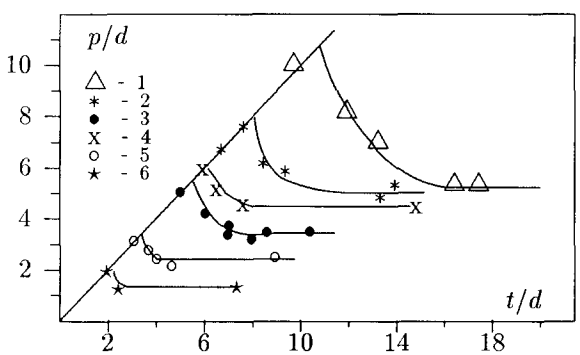

Fig. 3. Penetration depth p/d versus relative target thickness t/d.
1–3 - steel/STEF, 4 – steel/D16,
5–6 - glass/STEF.
V, km/s – d, mm: 1 – 11.2, 0.68; 2 – 7.5, 0.83; 3 – 4.8, 1.1; 4 – 7.5, 0.83; 5 – 7.8, 1.3; 6 – 2.8, 1.56.

perforated through or a small clearance is formed by through cracks, then $p/d = t/d$. The average value between two closest thicknesses, perforated and non-perforated one, was taken as the limit perforation thickness δ. Consideration of these results enables a quantitative concept of semi-infinite target to be introduced for which the cavern depth p is independent of the target thickness t. For tested material this thickness should not be less than $(7–15) \cdot d$ for the impact of steel projectile and $(3–5) \cdot d$ for glass projectile impact. When the target is thinner, the value p/d increases due to the action of the back surface rarefaction wave, as for duraluminium target: points with number 4 in Fig. 3 [6]. As the impact pressure increases, so does the region of p/d increase (the region of influence of back rarefaction wave). This is to a greater extent characteristic of the steel projectiles (points 1–3).

The character of target damage depends substantially on the material strength. For less strong ST-1 (Fig. 2a) the perforation near the limit is due to the closing of spalled hollow with the cavern bottom. This mechanism is analogous to that observed for strong metals. No spallation or macrodeformation of back surface (characteristic material buckling) are noticed for stronger STEF (Fig. 2b), which is determined by high values of deformability and tensile strength of reinforcing filaments. High elastic deformation energy in the material volume under the crater results in threshold character of perforation for STEF: there are no macrodeformations at the back target surface (except for the "whitening" discussed below); when the thickness is reduced by 0.5 to 1 mm, through perforation takes place.

The hole shape is somewhat similar to a circular cylinder. Its lateral surface is uneven. It is formed by the residues of glass filaments and hollows in the places where the matrix material poured out due to local nonuniformities in material density and strength. For the above reasons the hole diameter D may be estimated only as not exceeding $(1.5\text{–}2) \cdot d$.

In addition to the hole and failure in its vicinity the hypervelocity impact results in clearly defined "whitening" areas at both target surfaces (Fig. 1a). These "whitening" regions appear due to the binder material discontinuity caused by weak interlaminar strength and action of shear and tensile stresses initiated by joint action of the intense compression wave divergent from the impact point and rarefaction waves from the side of free surfaces.

As a rule, these regions are of elliptic form stretched along the glass fabric warp. Their characteristic area S ranges from 2 to 22 cm^2, which is much more than the cavern area (which is ≤ 0.1 cm^2). The "whitening" area is as follows: at back surface $S_b = 5$ to 22 cm^2, at front surface – $S_f = 2$ to 4 cm^2 at $t < \delta$. As the target thickness increases, the area of upper "whitening" increases slightly and peaks at $t \sim 2 \cdot \delta$, while the lower "whitening" area first increases, achieves maximum at $t \sim \delta$, and then vanishes to zero when $t \sim (1.5\text{–}2) \cdot \delta$. Therefore, when the target thickness increases, the equivalent diameter $D_{eq} = \sqrt{4 \cdot S/\pi}$ where S is half-sum of the "whitening" areas at front and back surfaces, first increases and peaks at $t \sim \delta$, then decreases to a constant value (Fig. 4). The growth of D_{eq} is due to the increase of projectile

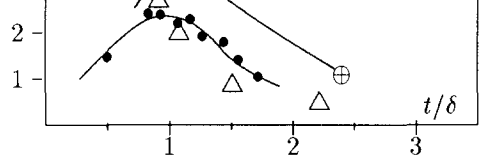

Fig. 4. The "whitening" equivalent diameter versus relative target thickness t/d at various projectile energy.
Projectile: 1 – steel, 3 km/s, 138 J;
2 – steel and glass, 4.8-7.8 km/s, 58-65 J;
3 – steel, 11.2 km/s, 87 J.

energy portion absorbed in the target, while its decrease may be explained by the reduction of shock wave intensity passing to the back side. For thick plates with $t > (1.5\text{–}2) \cdot \delta$ the whitening region appears only at the front surface (Fig. 1b).

Analogous damages in material structure with the impact energy in the range of 40 to 120 J are observed for both plates and tubes of graphite/epoxy plastics at hypervelocity impact [2, 3, 4], but no consideration was given to the thickness domain at $t \approx \delta$. Quantitative estimates of the sizes of these regions are of importance, since the elements of composites are used to support constructions and their partial failure at sufficiently large area may reduce significantly their admissible loads.

It should be noted that for steel/STEF the "whitening" region size was observed to decrease as compared to expected values at velocity 11.2 km/s and impact energy 87 J. In this case the target is likely to absorb the less portion of the striker energy or its lower part consumed for the "whitening" creation. No explanation has been found for this fact, but it correlates to the observed reduction of the crater depth in semi-infinite target.

The dependence of limit thickness on impact velocity is shown in Fig. 5. The strength of glass plastic is an essential parameter: when substituting STEF for ST-1 at $v = 4.8$ km/s, δ increases 1.5-fold for the material whose Brinell hardness is $\sim 70\,\%$ lower. This is likely to be

qualitatively stipulated by the change of damage character near δ (Fig. 2a): for ST-1 a spalled hollow is formed that interlocks with the cavern; spallation is not characteristic of STEF. The strength dependence of limit perforation is not characteristic of metals, and the increase of δ for harder, but more brittle material is connected with the influence of spallation [6].

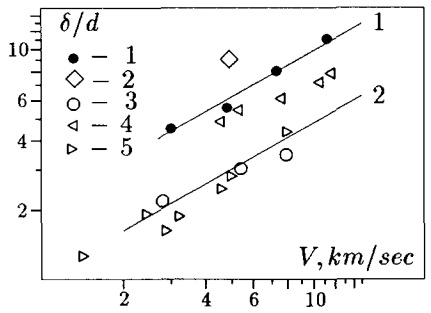

Fig. 5. The dependence of limit perforation thickness on impact velocity.
1 – steel/STEF, 2 – steel/ST-1,
3 – glass/STEF, 4 – steel/D16, 5 – glass/D16AT.

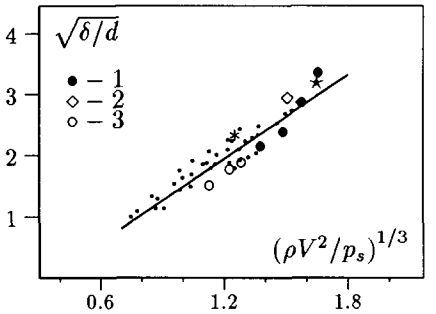

Fig. 6. Fitting of limit perforation data by Eqn (2).
1 – steel/STEF, 2 – steel/ST-1,
3 – glass/STEF.

If glass projectiles are used, the value δ decreases almost 2-fold as compared to the steel projectiles. Figure 5 presents analogous data for duralumin targets for comparison [6, 7]. It is evident that limit thicknesses are higher for the glass reinforced plastics impacted by the steel projectiles and are the same as for glass projectiles. This difference increases as the impact velocity of steel projectile grows. The ratio δ/p is ~ 1.5 for STEF, as well as for aluminum targets, when the spallings are insignificant. For the case of developed spalling this ratio increases up to 2–3 for metals [6]. Similar tendency is observed for ST-1 for which $\delta/p \approx 1.8$.

The data were fitted by the equation

$$\delta/d = K_t \cdot \rho^{\beta} \cdot v^{\alpha} \tag{1}$$

where ρ in g/cc, V in km/s and K_t is a constant for the target material. The Fish-Summers perforation formula [1] with $\alpha = 0.875$ inadequately describes the data for STEF composite. The perforation limit δ/d for steel projectiles varies better with impact velocity to the 2/3 power [6], line 1 in Fig. 5. The description of results for glass projectile impact on STEF-targets with the same value K_t but less projectile density and the values $\beta = 0.5$ (Fish-Summers formula) or $\beta = 1/3$ [6] typical for metals is failed. The stronger dependence on projectile density is needed for STEF-composite: $\delta/d \sim \rho^{2/3}$. Line 2 in Fig. 5 is built for the same value $K_t = 0.8$, but $\rho = 2.7$ g/cc. For less strong glass/epoxy composite ST-1 it is necessary to increase K_t up to 1.1.

Unified description of the results may be obtained in coordinates - $(\delta/d)^{1/2}$, $(\rho v^2/p_s)^{1/3}$ [8]. Here, the ratio of specific kinetic energy of the projectile to initial shock pressure in target p_s calculated by shock adiabats of projectile and target materials is taken as a parameter governing the perforation limit. Then the limit perforation of metals is approximated as follows

$$(\delta/d)^{1/2} = -0.76 + 2.26 \cdot x, \quad \text{where} \quad x = (\rho v^2/p_s)^{1/3}. \tag{2}$$

In Fig. 6 straight line is constructed from Eqn (2), points 1–3 are our results for glass/reinforced epoxy composites. Other points presents the data on the impact by steel and glass projectiles upon metals [6, 8]. The points for lead (asterisc) and magnesium (star) - metals with higher and lower investigated densities - are emphasized. Equation 2 fits the results for glass/epoxy composites reasonably well.

Thus, the following distinctions were observed for glass plastics as compared to metals: occurrence of additional areas of material damage; the limit perforation thickness depends on the material strength; the spallings are of low significance when the material is reinforced by two-directional glass cloth; the dependence of limit thickness on the projectile density is strong enough. At the same time for glass plastics the dependence of limit thickness on impact velocity may be fitted by Eqn (1) with $\alpha = 2/3$.

IMPACT UPON THICK TARGETS

For all materials, except for carbon/epoxy composite, the target thickness was sufficient to consider the target as semi-infinite. Because of their small thickness the carbon/epoxy plastic targets were placed on a thick bottom plate of building plaster to avoid the effect of rarefaction wave from its back side. This made it possible to eliminate the spallings under the impact of the projectiles whose diameter is no more than 1 mm (steel) and 1.5 mm (glass).

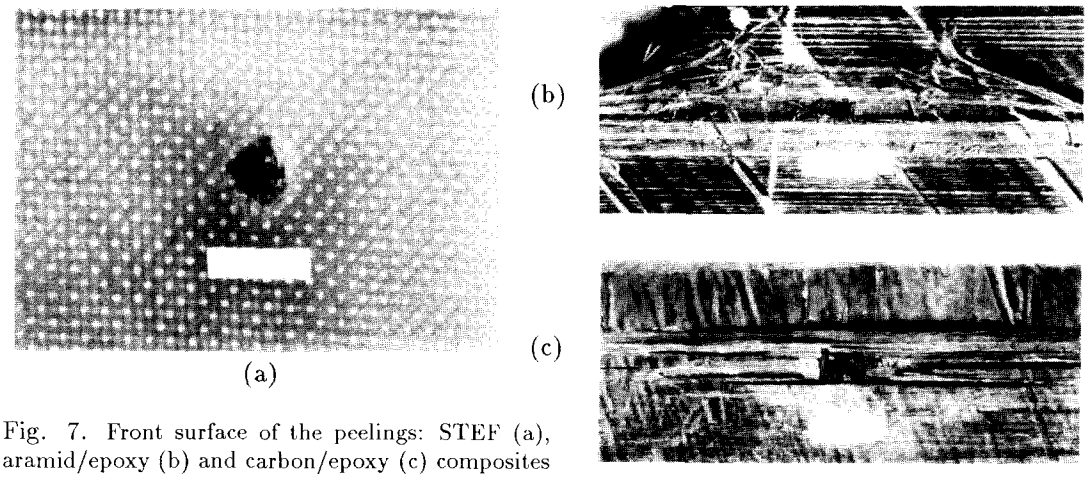

Fig. 7. Front surface of the peelings: STEF (a), aramid/epoxy (b) and carbon/epoxy (c) composites (steel projectile, 0.68 mm, 11.2 km/s; scale mark size - 1 cm).

Yew and Kendrick [2] showed that the cratering formation in carbon/epoxy system is accompanied by the front surface delamination and peeling under the action of shear stresses. It was shown that in the materials with unidirectionally arranged layers the direction of delamination coincides with the orientation of reinforcing fibers in the surface layer. When the material is reinforced by two-directional glass cloth, another damage pattern takes place. Figure 7 presents the front impacted surface of reasonably thick plates for tested composites. In all cases the projectile did not perforate the plates, there was no visual damage on the back surface of the plates.

The crater and peelings of the superficial laminae are observed at the impact surface of aramid- and carbon-fiber/epoxy targets. The direction of peelings is consistent with the fiber direction in the upper laminate and the peeling thickness is equal to the thickness of one upper laminae [2]. The length of peelings achieves 6 to 8 cm, and the width – 5 to 10 mm. In general the cavern area for carbon/epoxy is larger than for aramid/epoxy, and at higher velocity it was equal approximately to 7 and 4 mm^2, respectively.

The crater and the nearly circular symmetric specific damage zone, the "whitening" region, around the impact area were observed at the front surface of STEF-target. In the centre of this zone there is spalled material from the impact side. Its transversal size is $\sim (4 - 6) \cdot d$ and the spalling thickness is $\sim d$. This "whitening" region area S achieves $\sim$ 140 mm^2, and it is nearly forty five times larger than the cavern area ($\sim$ 3 mm^2), the impact area of projectile being only $\sim$ 0.5 mm^2. This may be compared to the impact on duraluminum D16 under the same conditions: the crater area is $\sim$ 23 mm^2, i.e. the maximum area of damaged material for the composite is 6 times larger.

When changing the striker kinetic energy E from 20 to 5230 J the "whitening" area of glass-textolite STEF increases from $\sim$ 0.5 to 18 cm^2. On the basis of 36 tests the "whitening" size for both steel and glass projectiles may be qualitatively described by means of formula $D_{eq} = (5.6 \pm 0.5) \cdot \sqrt[4]{E}$, where E in J, $D_{eq} = \sqrt{4 \cdot S/\pi}$ is the equivalent diameter of the damage area in mm (Fig. 8).

Stronger dependence of the diameter of the surface damage zone on the impact energy is

observed at through rupture of the carbon/epoxy composite with unidirectional fibers in separate layers : $D_{eq} \sim \sqrt[3]{E}$ [3]. This is undoubtedly due to the difference in reinforcement structure and test conditions: in the targets of finite thickness the lower "whitening" from the back target side (which is absent in semi-infinite targets) makes the greatest contribution to D_{eq}.

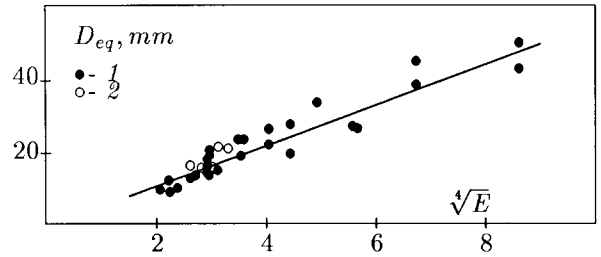

Fig. 8. The equivalent diameter of the front "whitening" area versus the impact energy for STEF.
1 – steel/STEF,
2 – glass/STEF.

Figure 9 presents the photographs of the sectioned craters formed by the impact of steel projectile on the targets made of aluminum alloy D16T (a), STEF (b), aramid-fiber/epoxy plastic (c), carbon/epoxy plastic (d) and epoxy (e). It is clearly seen that there is a significant difference in the size and shape of the craters: in elastic-plastic target their shape is close to hemisphere with characteristic ratio $p/D \sim 0.5$; in epoxy targets the elongated, circular simmetric cavern with $p/D \sim 2$ is observed; in composites the cavern are elongated, deep, noncircular symmetric with $p/D \sim 2$ to 4. The shape of the entry cavern in the plane is circular for aramid/epoxy and it is cross-shaped rather than circular for glass/ and carbon/epoxy targets (Fig. 7) because of anisotropy of material strength properties in the directions of reinforcing glass and carbon filaments. The cavern diameter D is equal to $\sim (1\text{–}2) \cdot d$ for STEF and aramid/epoxy plastics to the accuracy of $\sim (0.3\text{–}0.5) \cdot d$.

For carbon/epoxy plastic the cross-shaped structure is traced on the half of the crater depth and almost in the whole depth of crater under the impact of steel and glass projectiles, respectively. Hence the transverse size of the crater may be characterized by two values depending on a cutting direction: the first value is the maximum cross size $D_{max} \sim (3\text{–}4) \cdot d$; the second value is the diameter of about the circular region at the centre of the cross $D_{min} \sim (1\text{–}2) \cdot d$. In this case the relative depth of the crater $p/D_{max} \sim 0.7$ to 2 decreases and $p/D_{min} \sim 2$ to 4 remains as before. The observed peculiar shape is probably due to a rather large thickness of separate plys, the two-directional reinforcement and some post-effects of high brittleness of carbon filaments and low shear strength of material. The situation is somewhat similar to the impact upon brittle rocks for which "flattening out" of the crater is caused by the subsequent splitting phenomena on the side of the front surface of the target [9]. For glass-cloth-base composite the cross-shaped structure is observed only in one or two layers.

When the velocity of steel projectile is up to 11 km/s, the elongated crater with $p/D \sim 2\text{–}4$ is formed in all materials. This implies relative compactness of the striker material throughout the penetration process and weak radial flow of target material. Elongated shape of the caverns was

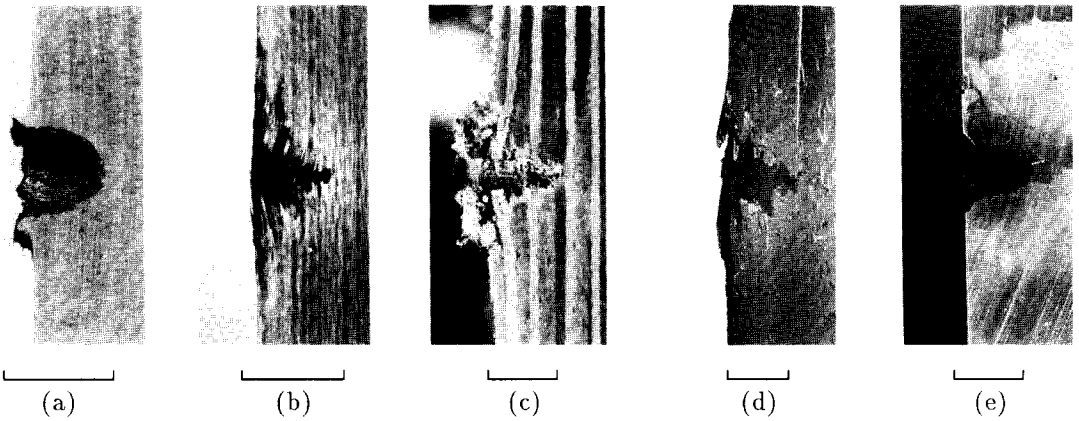

Fig. 9. The sections of through target craters (steel projectile, 0.68 mm, 11.2 km/s; scale mark size - 5 mm.). (a) – alloy D16; (b) – STEF; (c) – aramid/epoxy; (d) – carbon/epoxy; (e) – epoxy.

also noticed under impact of glass projectiles on STEF and aramid-fiber/reinforced composites. Elongated shape of the craters characterized by the ratio $p/D > 1$, cannot be completely explained by the difference in the densities of steel projectiles and targets ($\rho/\rho_t \approx 4.2$–6). Even in the case when glass particle strikes STEF-target ($\rho/\rho_t \approx 1.5$) at velocity 7.8 km/s, the cavern with $p/D \sim 2$ is formed. In less strong ST-1 textolite or carbon plastic the cavern occupies almost the whole volume of this zone, and cavern with lower p/D form.

Two peculiarities should be noted in addition to the decrease of relative crater depth for glass projectiles: 1) the contour of the second damage zone around the crater is nearly hemispherical; 2) entry crater diameter is larger than that of the craters made by steel projectile, $D/d \simeq 2$–4 at $v = 1.3$–7.8 km/s. Undoubtedly, the latter peculiarity is concerned with more intense failure of glass particle at the initial stage of penetration. Brittle glass particles break up even at the lowest velocities ~ 1 km/s. Therefore, the caverns with lower ratio $p/D \sim 0.7$–2.5 form.

For all of the materials, the layers below the cavern are almost not deformed. This indicates the absence of the stage of plastic flow which is characteristic of metallic targets and determines the final size of the cavern. The target material motion stops immediately after the consumption or stopping of the projectile whereas for metallic targets, additional plastic flow ensues.

The total loss of target mass Δm characterizing the portion of energy of steel and glass projectile required to destruct a part of target material has been determined. As well as for metals the results may be adequately described by the linear dependence $\Delta m/m_p \sim k \cdot v^2$, with coefficient $k = 0.58$ for STEF and $k = 1.3$ for ST-1 over the velocity range $v = 1$ to 8 km/s (m_p is the projectile mass, v in km/s). Let us assume that the volume V of failed material may be estimated as $V \sim \Delta m/\rho_t$. Then, the efficiency of crater formation may be estimated as $E/V \sim \rho_t/(2 \cdot k)$: $E/V = 1.55$ and 0.65 kJ/cc for STEF and ST-1 textolites, respectively. When the impact is directed "at butt-end" there are no spallings from the front surface, and the crater efficiency in this direction equals 1.45 kJ/cc at $H_B = 560$ MPa. For aluminium alloys E/V equals 0.4–2.1 [11].

The crater efficiency for a wide class of metal targets is described by the common Feldman dependence connecting E/V with Brinell hardness H_B of materials : $E/V = 2.6 \cdot 10^{-2} \cdot H_B$, where H_B in 10 MPa. The data for glass-textolites are in good agreement with this dependence, which is likely to result from the unity of the mechanism of projectile energy consumption in the target under hypervelocity impact independently of the material structure and properties. This fact is of interest because the morphology of forming cavern and its shape in metals differ considerably from those in the composites under test.

The dependence of the crater depth to projectile diameter ratio p/d as a function of the steel sphere diameter ranging from 0.9 to 4.5 mm for STEF-targets at almost constant impact velocity $v = 5$–5.5 km/s was obtained. When the steel projectile size decreases the reduction of cavern depth for about one gauge is observed. It was found that p/d scaled as the 1.13 power of the steel spheres diameter, i.e. $p/d \sim d^{0.13}$ (d in mm). This value of scaling factor agrees well with the observed exponent of the projectile diameter for the other materials, which ranges from 1.056 for ductile aluminum alloy to 1.2 for very brittle rocks and glasses [1].

Usually the diameter scaling is connected with the strain-rate dependence of target strength at the cratering formation phase and melting effects. From this point of view the glass-textolite with epoxy matrix is the appropriate representative of scaling effect due to the strong strain-rate dependence of compressive strength at dynamic compression [12] and low melting temperature of the matrix.

The dependences of p/d versus v for steel ($d = 0.53$ to 4.5 mm) and glass projectiles ($d = 1.3$ to 2.3 mm) are presented in Fig. 10 and 11 respectively. The data for epoxy resin are presented in Fig. 10. The matrix data are the upper limit for composites. The values p/d for composites vary widely, which is typical of mechanical tests on composites and is connected with randomly nonuniform mechanical properties of targets (even when cut from a single sheet of composite) and the inherently statistical character of reinforcing fiber damage. Despite this, a number of dependences are clearly defined. No consideration is given for the data at steel projectile velocity lower than 4 km/s, since in this case the well-known effects accompaning the penetration of

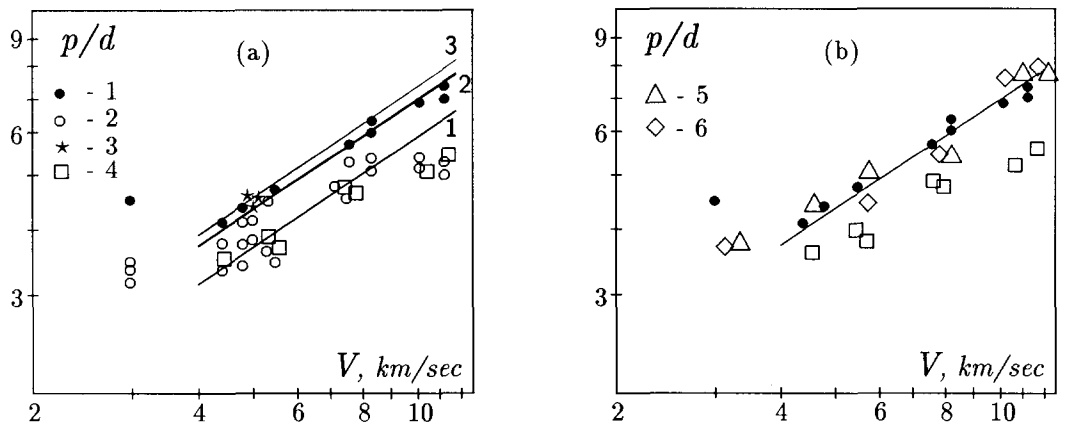

Fig. 10. Penetration depth to projectile diameter ratio versus velocity for steel projectiles.
1 – epoxy, 2 – STEF, 3 – ST-1, 4 – alloy D16, 5 – aramid/epoxy, 6 – carbon/epoxy.

strong undeformed projectile into the target with low shock impedance are the same as for metals disturbing monotonous increase of penetration depth as the velocity grows [13].

The formal approximation of the results for STEF and epoxy by the dependence $p/d \sim v^{\alpha}$ neglecting the projectile diameter scale effect yields $\alpha = 0.54$ and 0.59 respectively. With regard for the scale effect $\alpha = 0.73$ and 0.77, mean value of $\alpha = 0.63$–0.68. On this basis we selected the Charters-Summers formula with $\alpha = 2/3$ [14] in order to describe the dependence p/d on v for steel and glass projectiles and all target materials:

$$p/d = 1.5 \cdot (\rho/\rho_0)^{1/3} \cdot (\rho v^2/(2 \cdot S_t))^{1/3} \tag{3}$$

Here S_t is the dynamic strength resistance of target material to the projectile penetration which is determined from the approximation of experimental data by Eqn (3). This semi-empirical dependence is of interest, because it makes allowance for the effect of the target strength and the projectile density. Lines 1,2 in Fig. 10a are the least-squares fittings of experimental data by Eqn (3) at $v > 3$ km/s for steel/STEF and steel/epoxy impact. The respective fittings for aramid/ and carbon/epoxy composites (Fig. 10b) practically coincide with that for epoxy.

When using less strong material as a binder, for example, phenol-formaldehyde resin instead of epoxy, one should expect the increase of the cavern depth, other conditions being equal. Such an increase was observed for glass-textolite ST-1. Let us assume that substituting one matrix material for another one in glass-textolite, one may estimate the constant S_t considering it to be proportional to the Brinell hardness of the material H_B (static generalized strength characteristic of the target material). This assumption is based on the above mentioned correlation of crater formation efficiency with Brinell hardness. Then the estimate S_t for ST-1 will be : $S_{t,ST-1} \sim (H_{B,ST-1}/H_{B,STEF}) \cdot S_{t,STEF} = 16$ GPa. The decrease of S_t for ST-1 is connected with the lower strength of matrix. The line 3 in Fig. 10a is constructed from Eqn (3) for this value S_t. The agreement with experimental points for ST-1 is satisfactory.

The lines 1-3 in Fig. 11 are the formal prediction from Eqn (3) for the glass projectiles (other $\rho = 2.7$ g/cc) for the values S_t calculated using the data on the steel projectile impact upon the glass-, carbon- and aramid-fiber/reinforced epoxy composites. The agreement with empiric data is quite good. Note that according to Eqn (3) the crater depth p/d is proportional to $(\rho \cdot v)^{2/3}$.

So, the Charters-Summers formula allows one to estimate the influence of projectile velocity, its density and target strength for investigated composites, for the latter the value proportional to Brinell hardness of the target. Figures 10 and 11 show the analogous data for steel and glass projectiles and duraluminium targets [6, 7].

When the velocity of steel projectile increases up to 10–11 km/s ($d = 0.68$ mm) the cavern depth for STEF composite decreases approximately for one gauge with respect to extropolated data from the lower velocities (Fig. 10a). This decrease can hardly be explained by the influence of scaling effect, if, of course, it is not supposed that the size scaling factor increases as the

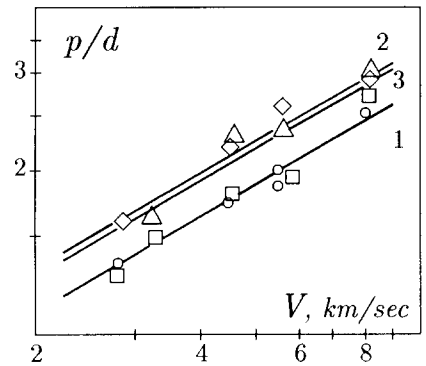

Fig. 11. Relative crater depth versus velocity for glass projectiles.
o - STEF, △ - aramid/epoxy,
◇ – carbon/epoxy, □ – aluminium alloy D16AT.

impact velocity increases. Additional effects are observed over this range of impact velocities: 1) blackening of the "whitening" regions from the impact side, 2) the cavern acquires clear conical entry, which indicates more intense ejection of target material (Fig. 9b), 3) the "whitening" equivalent diameter decreases during perforation of thin target (Fig. 4). The cavern entry diameter significantly increases up to $\sim 2.5 \cdot d$, and the cavern depth decreases to $p/D \approx 2$. Probably, the conditions necessary for evaporation of a part of binder at unloading are achieved, and the binder material decomposes with release of carbon as soot which retains in the volume of the front "whitening" region.

Analogous effect is not observed for of homogeneous epoxy resin, the cavern has the cylindrical form with $p/d \sim 7$ to 7.5 and $p/D \approx 2$ (Fig. 9e), although the deviation of points at 10–11 km/s down to approximation line is noticed (Fig. 10). This effect is not observed for either aramid- or carbon-fiber/epoxy composites (Fig. 11). The behavior of glass-textolite cannot be explained by the difference in shock pressure of the materials.

Perhaps, the reason is in different content of carbon per volume unit: in the case of glass-textolite it is 3–4-fold lower than for another materials. At high shock pressure ($\sim$ 1.5–2 Mbar) the physical condition, thermophysical characterictics and gasdynamic behavior of target material at unlouding may be determined by the high-pressure carbon phase and shock temperature of the composite components. The questions concerning the vaporization energy of physically and chemically inhomogeneous target medium in these conditions and the temperature of more compressed resin have not been solved accurately yet.

DISCUSSION

In our opinion the most characteristic peculiarities distinguishing the hypervelocity impact on laminated composite from that on homogeneous plastic metal are as follows: the emergence of surface peelings, elongated cavern shape characterized by ratio $p/D > 1$, and the dependence of the relative values δ/d, p/d on mass density and velocity projectile as $\sim (\rho \cdot v)^{2/3}$. These peculiarities may be related to the laminated structure governing the anisotropy of mechanical properties, the low target density, and the elastic-brittle deformation behavior characterized by high dynamic deformability up to 3–5% for glass- and up to 1.5–3% for aramid- and carbon-fiber/epoxy systems.

When using as a target magnesium, which is relatively plastic metal with density ρ_t = 1.74 g/cc, the impact of steel projectile ($\rho/\rho_t = 4.5$) with velocity equal 7.3 km/s (d = 0.83 mm) results in the elongated cylindrical cavern with $p/D \approx 1$ and $p/d \approx 5$. Under the same conditions the cavern in STEF-target ($\rho/\rho_t = 4.2$) has $p/D \approx 4$, $p/d = 5.4$. In the two cases the caverns are of close depth, but the cavern diameter in STEF is smaller, that is connected with dissimilar flow character of target medium under impact. The target made of composites can not show hydrodynamic flow due to the absence of the plastic section on stress-strain dependence. Additionally, the matrix melting behind the shock front (shock pressure $\sim$ 0.3 to 2 Mbar) may contribute to the cavern elongation.

The impact of steel projectile at 7.3 km/s upon the target made of the separate soft alu-

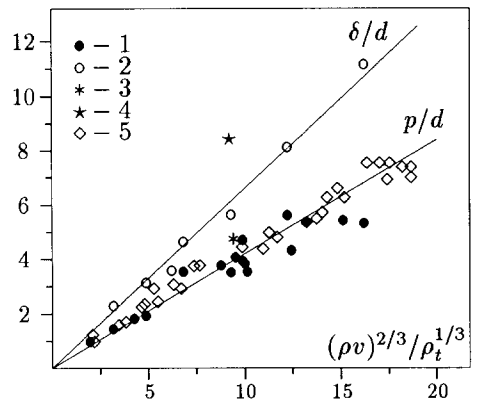

Fig. 12. Dependence of δ/d and p/d on parameter $(\rho v)^{2/3}/(\rho_t)^{1/3}$.
1,2 – STEF, 3,4 – ST-1, 5 – aramid- and carbon/epoxy composites.

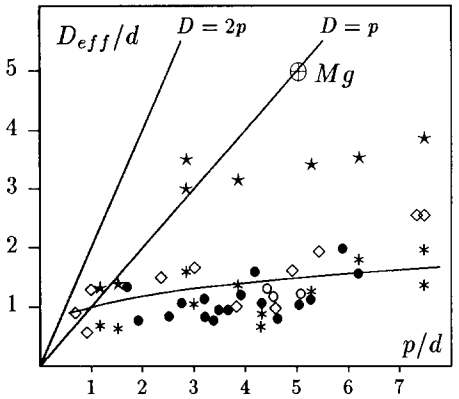

Fig. 13. Dependence of the cylindrical cavern effective diameter D_{eff}/d on p/d.
* – glass, • – steel projectiles.

minum foils glued together with thin layer of epoxy (the thickness of single foil equals to 0.12 mm) forms almost semi-spherical crater with $p/D \simeq 0.7$ and $p/d \approx 4$ (for homogeneous target - $p/D \approx 0.5$ and $p/d = 3.7$). There are the peeling of the several first layers on the impacted surface and the delaminations of some layers on the cross-section which are analogous to those observed in laminated glass-cloth base composite. Hence it follows that the observed peelings and delaminations in composites are connected with their lower interlaminar and peel strength which do not influence the formation of the crater itself.

The results of these qualitative experiments allow us to consolidate that the cavern lengthening for tested composites is their distinctive feature and is probably connected with their elastic-brittle deformation behaviour.

Let us show how the observed relation $(\delta/d, p/d) \sim (\rho \cdot v)^{2/3}$ may be connected with the fact of the cavern lengthening and week dependence of relative cavern diameter D/d on the impact velocity (or on cavern depth p/d). Assume that the function $D(p)$ has the form as $D/d \sim (p/d)^{\beta}$, for plastic metals and $\rho/\rho_t < 3$ it is $\beta \simeq 1$. Clearly, for discussed composites it is $0 < \beta < 1$. Then the volume of cylindrical part of observed central cavern may be estimated as $\sim p \cdot d^2 \cdot (p/d)^{2\beta}$. Let us suppose the volume of material ejected from this central cavern to be directly proportional to mechanical momentum of the projectile $m \cdot v$ (the reason for this is the subject of separate discussion going back to Walsh and Bjork, thus far there is no satisfactory answer to this question). Then we obtain $p \cdot d^2 \cdot (p/d)^{2\beta} \sim d^3 \cdot \rho \cdot v$, hence it follows $p/d \sim (\rho \cdot v)^{1/(1+2\beta)}$. From the analysis of experimental data it follows that $p/d \sim (\rho \cdot v)^{2/3}$, then $\beta = 1/4$, and for relative cavern depth and diameter we obtain the following equations

$$p/d \sim (\rho \cdot v)^{2/3} \tag{4}$$

$$D/d \sim (p/d)^{1/4} \tag{5}$$

Let us supplement Eqn (4) by the target mass density dependence ρ_t according to Charters-Summers equation as follows

$$p/d \sim (\rho \cdot v)^{2/3}/(\rho_t)^{1/3} \tag{6}$$

Assuming that $\delta \sim p$, and for δ/d we obtain the formula anologous to Eqn (6). Figure 12 shows the dependence δ/d, p/d on parameter $(\rho \cdot v)^{2/3}/(\rho_t)^{1/3}$ for all investigated impact conditions. The data are well fitted by straight lines. Figure 13 shows the results of measuring the cavern cylindrical part diameters in thick targets for all used materials in dependence on their depth: the straight lines are the approximations for ductile medium, solid curve line $D/d = k \cdot (p/d)^{1/4}$ is built for $k = 1$. There are presented two data sets (points $\star$, $\diamond$) for carbon-fiber/epoxy composite according to maximum and minimum cross-shaped cavern sizes in the above mentioned sense. Only the data on D_{max}/d (points $\star$) for carbon/epoxy composite drop out of the Eqn (5). The agreement for other data in Figs. 12 and 13 with functional estimates (5,6) is quite satisfactory.

Thus, application of the experimentally established fact of elongation, quasi-cylindricity of the caverns in laminated composites and of the assumption about the proportionality of the volume of cavern central part to the momentum of the projectile has two consequences expressed by Eqns (4–5) which describe experimental data quite well. In so doing, the target strength is not considered, of course, and the cavern lengthening is not explained.

CONCLUSIONS

At hypervelocity impact on laminated composites (glass-textolite, aramid-fiber/epoxy and carbon-fiber/epoxy composites) the reinforcement structure influences considerably the dimensions and character of additional damage zones on target surfaces. The area of these zones is much larger than the cavern area. The formation of these zones is connected with the laminated structure and the low interlaminar and shear strength of investigated composites.

The results obtained for glass-cloth-base composites with linen weave point to considerable influence of target material strength on limit perforation thickness which depends on the projectile density and velocity to power 2/3. Elongated cavern with rather complex structure depending on the target and projectile material are formed by steel and glass projectiles during the impact on semi-infinite targets.

The empirical dependences obtained earlier for metals such as the dependences of limit perforation on the projectile velocity and the crater efficiency on Brinell hardness, the influence of projectile size, its density and velocity on the crater depth in semi-infinite target may be used for estimation of the impact results for studied laminated composites. The peculiar shape of the caverns in the composites indicates that there is no stage of inertial plastic flow in forming the crater after the projectile is consumed or stopped, which is due to elastic-brittle deformation character of fiber reinforced composites.

Supported by the Russian Foundation for Fundamental Studies under contract No. 93-013-16499.

REFERENCES

1. B.G.COUR-PALAIS, Hypervelocity impact in metals, glass and composites. *Int. J. Impact Engng*, **5**(1–4), 221–237 (1987).
2. C.H.YEW and R.B.KENDRICK, A study of damage in composite panels produced by hypervelocity impact. *Int. J. Impact Engng.* **5**(1–4), 729–738 (1987).
3. E.L.CHRISTIANSEN, Investigation of hypervelocity impact damage to space station truss tubes. *Int. J. Impact Engng*, **10**(1–4), 125–133 (1990).
4. W.P.SCHONBERG, Hypervelocity impact response of spaced composite material structures. *Int. J. Impact Engng.* **10**(1–4), 509–523 (1990).
5. V.M.TITOV, YU.I.FADEENKO and N.S.TITOVA, Acceleration of solid particles by cumulative explosion. *Doklady AN SSSR (USSR)*, **180**(5), 1051–1052 (1968).
6. V.M.TITOV and YU.I.FADEENKO, Perforation under meteorite impact. *Cosmic investigations (USSR)* **10**(4), 589–595 (1972).
7. A.P.ANIKIEVA, L.A.MERZHIEVSKII and V.M.TITOV, Perforation of targets under impact of glass projectiles imitating stone meteorites. *J. Appl. Mech. and Techn. Physics (USSR)*, **3**, 131–136 (1977).
8. L.A.MERZHIEVSKII and YU.I.FADEENKO, Damage of thin-walled tubes filled with a liquid under meteorite impact. *Cosmic investigations (USSR)* **11**(6), 944–951 (1973).
9. V.M.TITOV, YU.I.FADEENKO and G.A.SHVETSOV, Hypervelocity impact on rocks. *Doklady AN SSSR (USSR)*, **191**(2), 950–952 (1970).
10. P.B.POND and C.M.GLASS, Metallophysical investigation and energy distribution. In *High-Velocity Impact Phenomena* (edited by R.Kinslow) ch.8, N.Y.& London (1970).
11. R.J.EICHELBERGER and J.H.KINEKE, Hypervelocity impact. In *High-speed Physics*, Wien-N.Y., Vol.2, ch.5 (1967).
12. A.V.PLASTININ, V.V.SILVESTROV and N.N.GORSHKOV, Dynamic compression of unidirectional fiberglass. *Dynamics of Continuum (in Russian)*, 93–94, 111–118 (1989).
13. A.E.WILLIAMS and M.A.PERSECHINO, The effect of projectile properties on target cratering. *Int. J. Impact Engng.* **5**(1–4), 709–728 (1987).
14. J.W.GEHRING, Hypervelocity impact from engineering viewpoint. In *High-Velocity Impact Phenomena*, (edited by R.Kinslow) ch.9, N.Y.& London (1970).